JOURNAL OF ENGINEERING SCIENCES

Volume 11, Issue 2 (2024)

Cioroagă B. D., Cioată V. G., Socalici A. V., Linul E., Hulka I., Anghel I. M. (2024). Optimization of submerged arc welding through voltage variation to achieve superior mechanical properties using P355N base material. Journal of Engineering Sciences (Ukraine), Vol. 11(2), pp. C42–C56. https://doi.org/10.21272/jes.2024.11(2).c4

Optimization of Submerged Arc Welding through Voltage Variation to Achieve Superior Mechanical Properties Using P355N Base Material

Cioroagă B. D.[1][0000-0001-9282-7264], Cioată V. G.[1*][0000-0002-5578-2308], Socalici A. V.[1][0000-0002-1854-882X], Linul E.[2][0000-0001-9090-8917], Hulka I.[3][0000-0001-5442-0631], Anghel I. M.[2][0009-0006-0197-2719]

[1] Faculty of Engineering in Hunedoara, Politehnica University Timişoara, 5, Revoluţiei St., 331128, Hunedoara, Romania;
[2] Faculty of Mechanical Engineering, Politehnica University Timişoara, 1, M. Viteazu blvd., 300222, Timişoara, Romania;
[3] Research Institute for Renewable Energy, Politehnica University Timişoara, 138, G. Musicescu St., 300774, Timisoara, Romania

Article info:
Submitted: August 22, 2024
Received in revised form: November 2, 2024
Accepted for publication: November 6, 2024
Available online: November 12, 2024

***Corresponding email:**
vasile.cioata@upt.ro

Abstract. This study focuses on the optimization of the submerged arc welding (SAW) process through the variation of welding voltage to achieve improved mechanical properties of butt-welded joints made from P355N fine-grained low-alloy carbon steel as a material commonly used in the production of pressure vessels. The optimization process was carried out by analyzing the effects of different welding voltages on mechanical performance, including tensile strength, hardness, and metallographic characteristics. In addition to mechanical testing, the study evaluates weld geometry and the transition zones to provide a comprehensive understanding of how voltage variation can optimize the welding process and improve joint performance. The welded samples were obtained using five different welding modes, the primary variable of which was the intensity of the welding current with a voltage range of 22–38 V within a seemingly narrow range. Significant changes were identified in microstructure, mechanical properties, and the shape and size of the welded joints. The experimental samples were considered from welded joints made from 6 mm thick plates of P355N material. The reference criterion against which the welding modes under study were compared is the industry-standard welding voltage of 33 V.

Keywords: welding, process innovation, voltage, hardness, structure, strength.

1 Introduction

In the pressure vessel (PV) manufacturing industry, submerged arc welding (SAW) is typical for making continuous joints on straight or circular welding paths necessary for closing and sealing vessels. The welded joints used to obtain the closed shapes of the PVs should meet a series of operational conditions, such as tensile stress, fatigue, tightness, and corrosion resistance. In order to ensure the best operating properties of the PV, appropriate welding processes and modes should be used.

Dedicated base material is also required to withstand the operating conditions that may consist of high temperatures and pressures and the environment created by the substances stored in the PV [1].

In the case of PVs as railway wagons used for the transport of various petroleum products, they are made of semi-finished steel profiles and sheets. The material of the semi-finished products consists of structural steel for the chassis part, cast iron for the bogies part, alloy steel for the gears, and PV steel for the vessel body. Most of these parts that make up the wagon vessel are assembled by welding processes. The vessel assembly consists of two parts: the vessel shell, the central shell, and the end caps.

The central part of the PV is made of a rolled sheet and closed by a longitudinal welding seam, forming a cylindrical tube at the ends of which two caps made of embossed sheet metal are mounted, their assembly being done by welding on a circular contour.

The welding method used to join the parts that make up the shell of the PV is SAW, which is preferred due to its high productivity. Through this method, long and continuous welding seams are efficiently executed. As a result, the joints are usually butt-welded [2–4].

2 Literature Review

Studying the effects of welding mode parameters for various welding technologies and various combined materials has always presented an area of interest for research and industry, as evidenced by the many scientific research papers published in this regard. Parameters such as welding speed, amperage, and welding voltage on mechanical properties and chemical composition are addressed by Kanjilal et al. [5], where SAW was the analyzed welding method.

Ahmad et al. [6] dealt with parameter optimization aspects in SAW processes (voltage, electrode feed rate, amperage, electrode extraction, and travel speed) based on statistical data.

The effects of the variation of welding process parameters on the microstructure of welded joints were studied by Zhang et al. [7]. For welding Q355B steel, the authors used laser arc hybrid welding and found that the large amount of martensite formed in the heat-affected zone (HAZ) led to higher hardness values for the weld area.

Assefa et al. [8] investigated the joining of low-carbon steel parts using welding technologies with a protective environment of inert gases. In order to obtain higher qualities of the welded joints, they varied the parameters of the welding modes.

Also, aspects regarding both the improvement of the quality of the welds and the economic part of the welding processes were reported by Habba et al. [9].

Recently, Ziółkowski et al. [10] paid more attention to the welding technologies of aluminum parts using Friction Stir Welding (FSW). The authors varied the process parameters and studied their effects on the microstructure, hardness, and tensile behavior.

Studies in the field of PV welding using the technology of SAW and materials in the category of PV steels have also been reported in the research works [11–14]. The first type of investigation highlights the effect of different welding voltage stages on the dimensions and geometry of the welded joints, identifying direct correlations between the welding voltage increase and the evolution of the dimensional parameters of the welded joints.

More approaches regarding welding seam geometry and dimensions related to the welding voltage and other SAW parameters effect can be found in research works [15–17]. These researchers address issues regarding the effect of gas metal arc welding on the groove shape of the molten metal flow. This research uses a computational model to describe the behavior of the melt pool and the effect of the groove shape.

Murugan and Gunaraj [18] presented ways to control and predict SAW weld bead geometry, presenting the experimental and statistical basis for the realization of a control and optimization system using variable parameters that affect the weld joint's geometry.

Manonmani et al. [19] investigated the geometry of welded stainless-steel sheets using laser beam welding technology.

Welding in ultra-narrow gaps using visual measurement methods that inspect the weld cross-section geometric dimensions was studied by He et al. [20]. The design of their model for the fulfillment of measurements is based on experimental tests that observe the variations in dimensions and geometry of the welded joints based on welding process parameters.

Aspects regarding the micro-hardness distribution in the cross-section of the welded joint are also found in research worldwide. Particularly, Dong et al. [21] studied how welding speed affects hardness and microstructure in friction stir welding joints of 6005A-T6 aluminum alloy. The authors found that the hardness of the nugget zone depended on the level of natural aging at different welding speeds, and the HAZ expanded as the welding speed decreased. They also found that Q-type precipitates have the most significant influence on the HAZ.

Gharibshahiyan et al. [22] used inert gas welding to investigate the effect of amperage and voltage on the microstructure and hardness of low-carbon welded steel. The authors obtained that as the amperage and voltage increase, the mechanical properties of the welded joint decrease at the microstructure level. In addition, they noted that increasing the welding voltage leads to an increase in grains in the HAZ.

Singh et al. [23] identified ways to optimize SAW processes using experimental data, such as the welded joints' hardness evolution depending on the welding mode parameters (welding current, welding voltage, wire feed, and carriage speed). Experimental data was used to train a C++-based expert system and neural network that can predict the effects of the previously mentioned welding parameters on the hardness of the welded joints, performing an analysis that results in an optimal welding modes adapted for different situations.

The analysis of metallographic microstructures in different areas of the cross-section of welded joints has received some attention from researchers. Investigations on the microstructure of SAW joints were carried out by Küçüköner et al. [24]. They made welded joints of duplex stainless steel AISI2205 with pressure vessel P355 GH as base materials and used as flux material ELIFLUX BSS-A together with the filler material consisting of 3.2 mm diameter welding wire ELOX 309 L.

From the analysis of the microstructure of the welded joints, the presence of a dendritic structure with a coarse grain shape was found in the transition zone from the weld to the base material. Investigations on the correlations of the SAW process parameters with the microstructure evolution in the welded joint area are presented by Lan et al. [25]. The authors have summarized a series of scientific papers, following which they have elaborated conclusions regarding the effects of process parameters (e.g., welding voltage, welding current, welding speed, wire diameter, granular flow) on the microstructure. They concluded that by increasing the arc voltage, the SAW method ensures the formation of ferritic structures in proportions above 4 %.

The novelty of the research consists of forming a complete image of the evolution of the welded joints' quality using SAW technology to determine welding

modes that offer superior mechanical properties compared to the standard welding mode currently used in the industry for welding PV made from base material P355N.

Also, an important aspect is the correlation of the welding voltage with the results of tensile tests, microhardness, and microstructure analysis to make future predictions about the weld quality and how it can be optimized by varying the welding voltage parameter. The results of this research correlated with other investigations regarding other parameters of the SAW process, such as the welding current, the welding speed, and the angle of inclination of the electrode, which can lead to the achievement of a much more precise optimization of the welding modes used for the fabrication of PV.

3 Research Methodology

3.1 Materials

Only two levels of headings should be used. Lower-level headings remain unnumbered. The materials used for conducting experiments are some of the industrial applications frequently found in the construction industry of pressure vessels. The materials can be classified into three large categories: the basic material, the filler material, the material with a protective environmental role, and the flux material. All of them were procured from the Reva railway tank wagon factory in Simeria (Romania), where the experimental samples were developed.

The basic material used to make the welded joints using different welding modes in which the welding voltage parameter was variable is carbon steel, a low alloy with fine grain, specially designed for making pressure vessels that work at high pressures and temperatures.

According to the specialized source [26], the basic material is P355N. Its naming and coding are regulated by the standard EN 10027-1:2005. This material also has specific characteristics: the preservation of mechanical properties in high temperatures, good plastic properties, easy processing by cold plastic deformation, and suitable weldability properties.

Within the standard SR EN 10216–3:2014, aspects regarding the family of which the basic material P355N is a part are dealt with, and its chemical composition and mechanical properties [27] are presented compared with other materials in its group. The base material used is a sheet laminated and normalized with a thickness of 6 mm, used in the process of making the railway tank wagon vessel covers.

In the case of the filler material used, this is a consumable electrode wire with a diameter of 3.2 mm, being specially intended to be used in welding processes that use submerged electric arc welding technology. The electrode is made from molybdenum-alloyed steel with copper clothing material ESAB OK Autrod 12.24.

Table 1 shows the chemical composition of the base material and the filler material.

Table 1 – Chemical composition of the welding base material and the filler material, % [27, 28]

Alloying element	Base material		Filler material	
	P355N		OK Autrod 12.24	
	min	max	min	max
Carbon [C]	–	0.20	0.08	0.12
Silicon [Si]	–	0.50	0.05	0.20
Manganese [Mn]	0.90	1.70	0.95	1.20
Phosphorus [P]	–	0.025	–	0.02
Sulfur [S]	–	0.02	–	0.02
Aluminum [Al]	–	0.02	–	–
Chromium [Cr]	–	0.30	–	–
Copper [Cu]	–	0.30	–	–
Molybdenum [Mo]	–	0.08	0.45	0.60
Niobium [Nb]	–	0.05	–	–
Nickel [Ni]	–	0.50	–	–
Titanium [Ti]	–	0.04	–	–
Vanadium [V]	–	0.10	–	–

The flux type material ESAB OK Flux 10.72 is intended for welding with electrode wire using high intensities of the welding current. The flux material plays a critical role in the welding process. It fulfills the function of a protective environment, preventing the communication of the welding bath with atmospheric gases, preventing the release of gases and light due to electric arc burning, and facilitating the slow cooling of the welded joint. The flux is a granular material of agglomerated type, which in this case has a density of 1100 kg/m^3 and a grain size included in the interval 0.32–2.0 mm [28].

3.2 Manufacturing process

The SAW machine used to weld the plates is semi-automatic from the industry used for welding the vessels that make up the railway tank wagon. The welding machine comprises the mobile beam, the power source, and command-and-control devices for the parameters of the welding mode.

A torch is installed at the end of the mobile beam, and the flux type material deposition system, flux type material collection system, and electrode wire feeding system are installed (Figure 1).

Before the execution of the welded plates, the semi-finished products consisting of a 6 mm thick sheet from material P355N were brought to 600 mm long and 125 mm wide plates. The guillotine cutting method was used to bring the plates to the desired dimensions, and the edges to be welded were cleaned with polishing to remove oxides.

The plates obtained were fixed end to end by applying four welding points, maintaining a gap of 1 mm between them (Figure 2 a).

The last stage in the preparation of the welding material is the application of a ceramic strip over the welding joint, which will have the role of supporting the root of the weld during the welding process in order to avoid leakage of filler material, the ceramic strip with adhesive wings (Figure 2 b).

a b c d

Figure 1 – SAW equipment used for the preparation of welded samples: a – end beam; b – mobile beam; c – control unit PEK-ESAB; d – power source LAF 613-ESAB

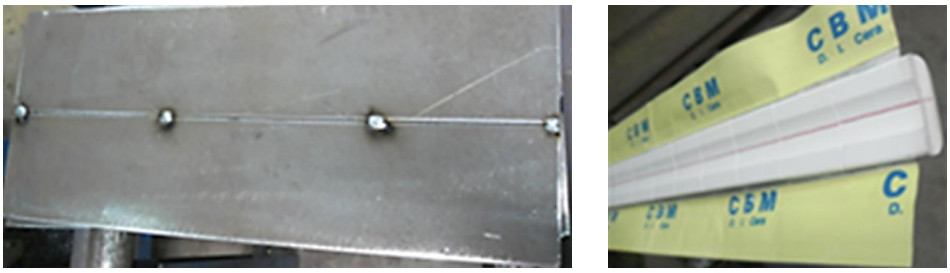

a b

Figure 2 – The base material prepared for welding the samples: a – plate; b – ceramic strip.

The welding mode considered standard, which serves as the reference base for the experimental findings, is the welding mode used in the industry, which is defined by the following parameter values: welding voltage – 33 V; welding current – 480 A; welding speed – 60 cm/min; the tilt angle of the electrode – 90°.

In addition to the parameters common to electric arc welding methods previously mentioned, the process characteristics should be mentioned, such as the welding under flux with wire electrode according to standard EN ISO 4063 and codification according to the standard [29].

According to standard SR EN 287–1 for butt welding with full penetration, the joint type is under coding BW [30]. Also, there is a one-pass welding, having the codification SL.

According to standard SR EN ISO 6947, the welding position is horizontal; it has the codification PA [31]. Also, the height of the deposited flux material layer is about 25 mm.

The welding modes under study modify the standard welding mode by assigning different values to the welding voltage parameter and the other welding parameters and conditions remaining constant. The welding voltages that define the observed welding modes have the values of 22, 26, 30, 34, and 38 V.

Welding the samples begins by fixing the plates in the position of the plates intended to be joined by SAW. The torch of the welding machine is brought to the welding position. The first stage is the flux layer's deposition, followed by the electric arc starting under this flux layer. Welding occurs on a straight path at a constant speed

maintained throughout the welding process. The distance between the tip of the electrode wire and the welding surface is kept constant throughout the welding process, as is the perpendicularity of the electrode to the welding surface. The electric arc that burns under the flux layer melts the electrode and partially the base material, filling the welding joint with a liquid pool of molten metal that solidifies over time due to cooling.

Approximately 200 mm behind the electrode is a system for suction and recovery of the flux layer that leaves behind the welded cord on the surface, where a crust of slag will be removed by gently tapping with a rigid tool.

In Figure 3, the stages of the process of welding the samples can be observed.

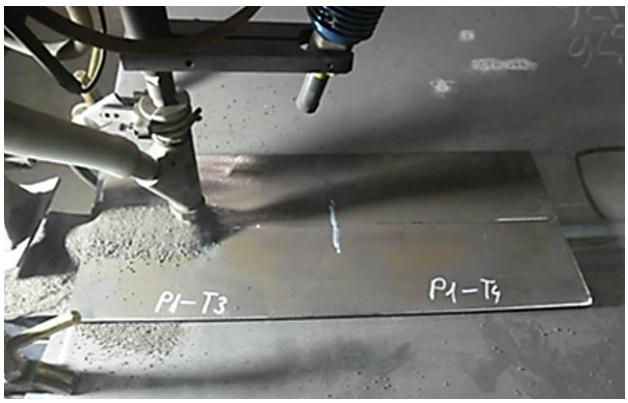

Figure 3 – The SAW process of samples

The length of a welding seam with a particular welding mode is 300 mm. On a set of plates, two different welding modes are found. As a result of the welding process, three whole welded plates resulted, which in total treated five welding modes.

Figure 4 shows the samples made using the preset welding modes with specific welding voltages of 22, 26, 30, 34, and 38 V.

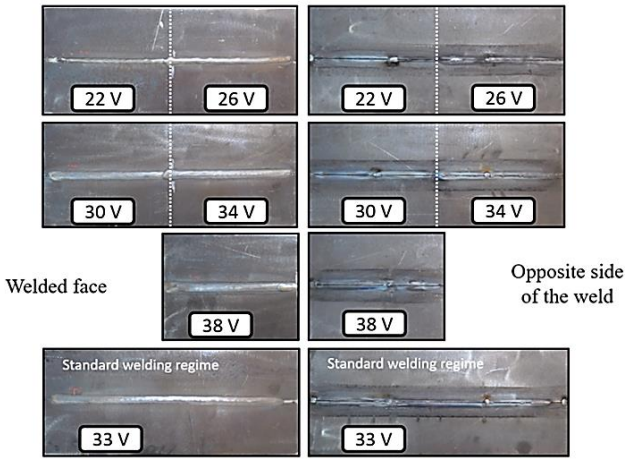

Figure 4 – Welded samples

Significant visual differences can be observed on the welding seams regarding width, elevation, and thermally affected area. The thermally affected area can be better observed on the opposite side of the welding face, where it is also possible to observe the penetration of the filler material into the welding joints [32].

Three specimens were extracted from the plate welded samples for tensile testing from each plate. The sampling of the samples for the tensile test was carried out by cutting three strips from the main plate by guillotining. Later, the strips obtained were processed by milling to obtain the sample breaking area. The shape and dimensions of the sample, as well as the sampling method, were made according to the standard BS EN 895:1995 [33].

Figure 5 shows the shape of the tensile test specimen and its dimensions in millimeters.

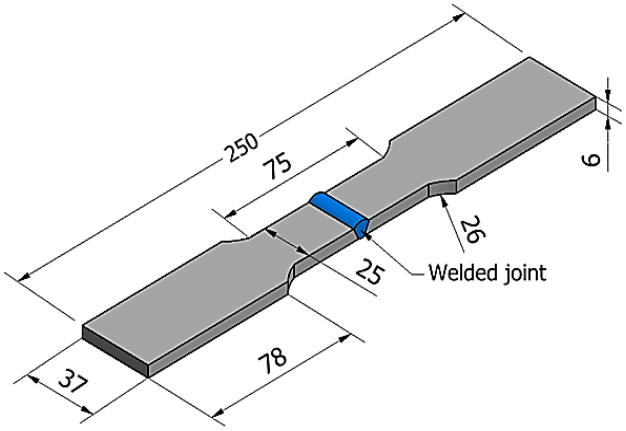

Figure 5 – Tensile test specimen according to the standard BS EN 895:1995 [33]

The tension test involves the application of a transverse stretching force on the welded joint. The load is progressively increased by 50 MPa/s until the specimen suffers a fracture.

3.3 Experimental setup

The transverse tensile tests of the welded joints were performed on the A009 (TC100) universal testing machine with a maximum load-cell capacity of 100 kN. The tensile test involves the application of a transverse tensile force, normal to the welded joint until the specimen undergoes a fracture. The tests were performed at room temperature, and the loading was applied quasi-statically at 50 MPa/s.

An extensometer was used to determine the modulus of elasticity. The extensometer was fixed on the test specimen to cover the weld joint fully. Depending on the failure area (in the weld joint or outside), the samples showed more or less plastic deformation. However, regardless of the area of the failure and the welding joint manufacturing conditions, the samples showed a ductile fracture.

The part of the study that deals with aspects related to the effect of welding current voltage on the hardness of the welded joints was carried out using a Wolpert 402MVD hardness tester equipped with a Vickers intender.

Samples for Vickers hardness testing were taken from the welded plate by sawing. The cutting took place with continuous cooling with oil so as not to affect the cutting area thermally. The Vickers indenter was a diamond pyramid with a square base featuring an angle of 136° between opposite faces, which is standard for such

hardness measurements. A load of 10 N was applied for a dwell time of 10 s during each indentation to ensure consistent penetration depth and measurement accuracy.

After processing the samples to bring them to a reasonable size, they were embedded in the resin and polished on the side on which the hardness measurements were performed. After a mirror gloss was obtained by polishing, the surface of the samples was attacked with a reactive solution to highlight the thermal transition zones of the weld.

The welded joints were examined in cross-section by scanning electron microscopy (SEM) – Quanta FEG 250 using a secondary electron detector in high-vacuum mode at an acceleration voltage of 15 kV.

Before the investigation, the standard ASTM E3-11 was employed to prepare samples. The samples were cut from the welded seam, grinded with emery paper from 280 to 4000 grit size, and then polished with 0.1 μm alumina paste on a polishing pad until a mirror-like surface was reached. Afterward, the samples were cleaned with acetone in an ultrasonic cleaner and etched using Nital reagent.

The metallographic samples are presented in Figure 6, which shows a degree of penetration of the filler material into the welding joints.

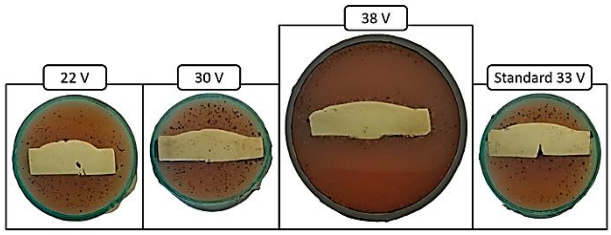

Figure 6 – Samples used for metallographic investigations

4 Results

4.1 Tensile results

Following the tensile tests, the force-displacement data were obtained [34, 35]. Using the cross-sectional dimensions of the samples and the indications provided by the extensometer, they were converted into stress-strain curves. Thus, three characteristic curves were obtained for each of the 6 voltage modes (22, 26, 30, 33, 34, and 38 V).

Figure 7 compares the stress-strain curves using the most representative curve from each voltage mode.

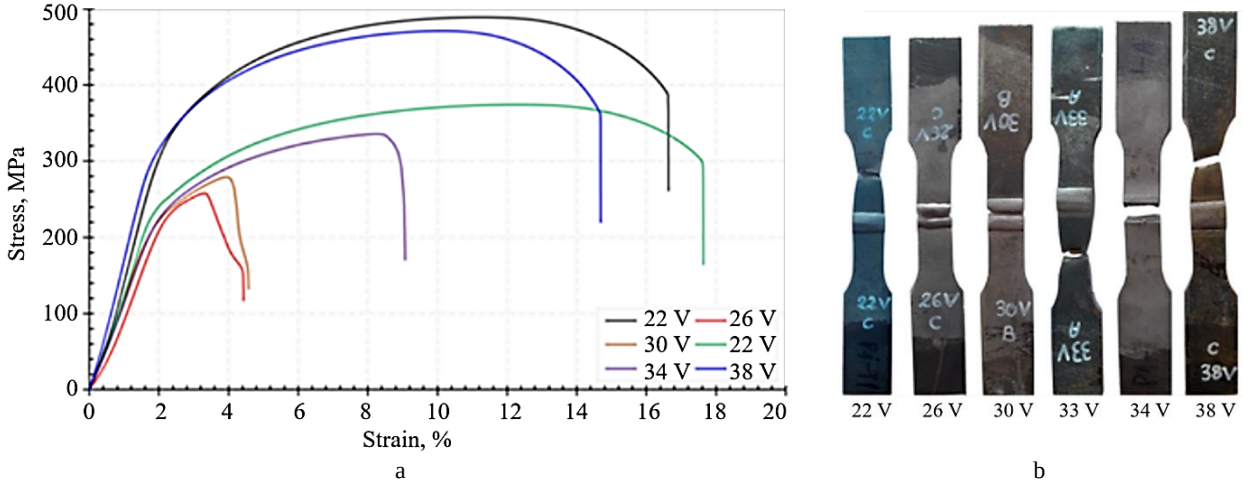

a b

Figure 7 – Stress-strain curves (a) and fractured samples (b) for different welding modes

The voltage value of 33 V is considered standard welding mode, so all these will be compared with this. The characteristic curves show that the tensile stress-strain curve of the standard welding mode (33 V) is in the middle position compared to the other studied welding modes. The development of characteristic curves at higher values of stress and strain indicates a weld-ed joint with high properties (e.g., stiffness and strength) [36].

Figure 7 shows that two welding modes (22 and 38 V) lead to mechanical characteristics superior to the standard mode (33 V). Both in terms of stress and strain, the 22 V mode is slightly superior to the 38 V mode.

It is also observed that the 22 and 38 V modes present an increased ductility of the samples, however slightly lower than the standard mode.

The specimens obtained with these modes break outside the weld joint. At the opposite pole, the 26, 30, and 34 V voltage modes show the lowest mechanical behavior, with a fracture of the specimens in the weld joint.

The specimens show a yield zone and a quasi-brittle fracture [37]. The samples obtained with 2 V have the lowest tensile properties among the three modes.

After processing the data from Figure 7, the tensile properties of the welded joints were determined.

Table 2 summarizes the main tensile properties of the tested samples. However, not all of these characteristics determine the optimal welding mode. The main ones to consider are maximum stress (tensile strength) and yield stress [36].

Table 2 – Main material properties obtained from tensile tests

Average property	Unit	Voltage, V					
		22	26	30	33	34	38
Modulus of elasticity	MPa	112 253	111 450	127 883	145 953	148 840	143 043
Yield stress	MPa	276.82	137.38	208.98	235.54	215.36	313.92
Strain at yield stress	%	1.85	1.43	1.88	1.73	1.94	1.89
Maximum stress	MPa	485.83	249.75	273.39	368.5	318.75	470.70
Strain at maximum stress	%	11.07	3.57	3.83	10.83	6.40	10.15
Stress at break	MPa	325.47	116.72	135.65	173.26	159.71	220.82
Strain at break	%	15.71	4.83	4.51	15.71	7.20	14.78
Fracture energy	kJ	6478	720	834	4942	1712	5903

Figure 8 shows the variation of stresses (yield stress, maximum stress, and stress at break) depending on the welding voltage mode (22–38 V). It can be seen that the 22 and 38 V welding modes highlight the highest values for all stresses. The strength properties for the 22 V mode (276.8 MPa for yield stress, 485.8 MPa for maximum stress, and 325.5 MPa for stress at break) are superior to 38 V for maximum stress (3 %) and stress at break (47 %), respectively lower for yield stress (13 %). Comparing the nominal values (33 V) with the maximum values (22 V), 18, 32, and 88 % increases are obtained for yield stress, maximum stress, and stress at break properties. The worst strength properties are found for the 26 V mode. The values given by the 26 V welding mode are lower than the ideal one (22 V) by 95 % for maximum stress and up to 178 % for stress at break.

According to Figure 9, the strain properties (strain at yield stress, strain at maximum stress, and strain at break) also present significant differences between the investigated modes (22–38 V).

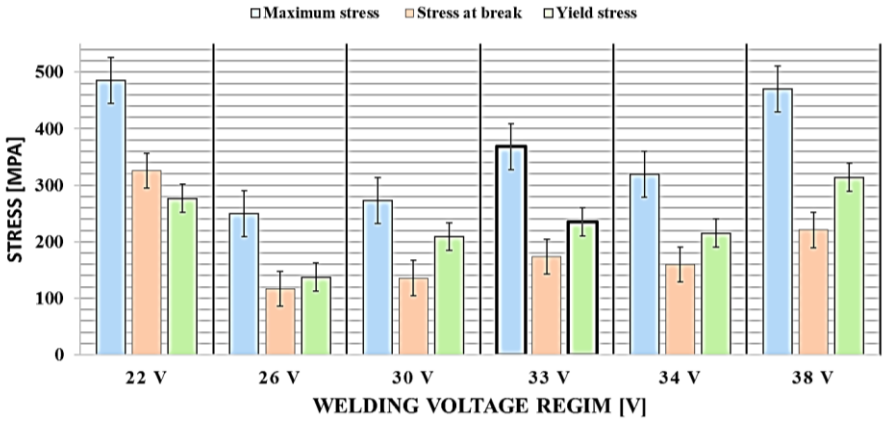

Figure 8 – Variation of stresses with the welding voltage mode

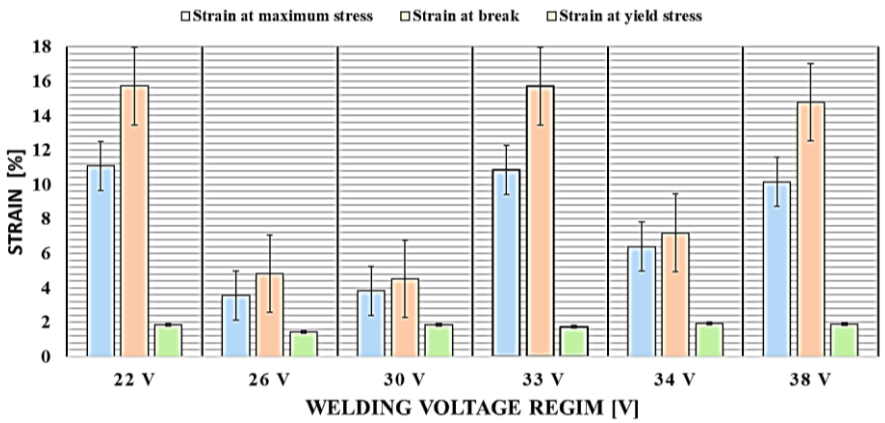

Figure 9 – Variation of strains with the welding voltage mode

Similar to the stresses, the highest strain values are exhibited by the 22 V mode. However, this time, the differences between the maximum and nominal values are much more minor. Thus, the 22 V welding mode outperforms the 33 V mode by 2 % (strain at maximum stress) and 7 % (strain at yield stress) in deformations.

It was obtained that strain at break shows the same average value for both welding modes. Regarding the

minimum mode (26 V), it shows values of strain properties up to 211 % (strain at maximum stress) and 225 % (strain at break) lower than the high-performance mode (22 V).

Due to the shape of the stress-strain curves and the superior mechanical behavior, the specimens manufactured with the 22 V welding mode have a fracture energy 31.1% higher than the nominal mode (33 V) and 799 % compared to the most unfavorable one (26 V).

The 34 V mode shows the highest modulus of elasticity ($1.49 \cdot 10^5$ MPa). The 26 V mode shows the lowest modulus of elasticity ($1.11 \cdot 10^5$ MPa). Thus, a percentage difference between the two values of 34 % is obtained.

4.2 Hardness results

To determine the effect of the welding voltage on the hardness distribution in the cross-section of the welded joint as well as the microstructure, measurements, and observations were made in six different areas of the cross-section of the welded joint (Figure 10).

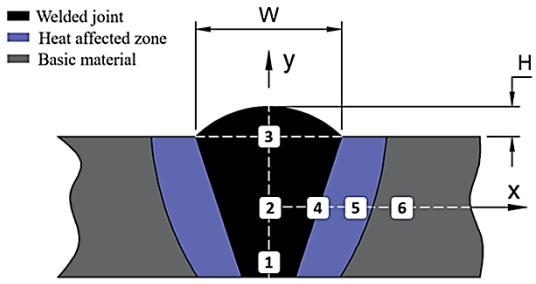

Figure 10 – The areas subject to hardness testing and metallographic inspection of the specimens' welded joints

The hardness distribution in the cross-section of the welded joint was analyzed using two hardness measurement directions: a vertical direction indicated by the y-axis and a horizontal one on the x-axis. For the dimensional analysis of the welding seam, the width dimensions of seam *W* and the height dimension *H* indicated in Figure 10 were considered.

The area indicated with point 1 represents the bottom root of the weld, the area with the weakest penetration of the base material in the welding joint. Point 2 represents the middle zone of the weld, being the area that benefited from the slowest cooling and complete penetration of the weld. Point 3 is at the level of the surface on which the welding was performed, which is the widest area of the cord section. Point 4 is located in the transition zone of the weld to the base material on the welded side. Points 5 and 6 are located in the cross-section of the base material, point 5 is located in the heat-affected zone, and point 6 has common properties for all analyzed situations, this being the pure base material.

The measurements to determine the Vickers hardness distribution in the cross-section of the weld bead were made by measuring four times the hardness in each of the six areas shown in Figure 10, the data with which the hardness is presented graphically as the average of these measurements.

Figure 11 presents the hardness distribution along the X-axis.

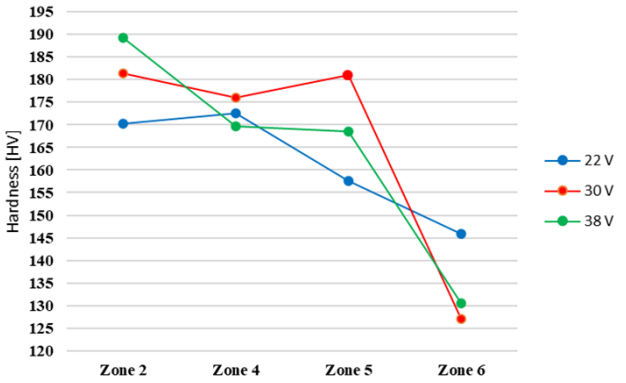

Figure 11 – Hardness distribution in the cross-section of the welding seam on the X-axis

Hardness decreases progressively from zone 2 to zone 6, regardless of the welding voltage applied. For all three welding voltages (22, 30, and 38 V), the highest hardness values are recorded in zone 2, corresponding to the weld's central part. As we move further from the weld toward the base material, there is a marked decrease in hardness, with the lowest values seen in zone 6.

The results indicate that higher welding voltages, particularly 38 V, lead to a more significant and rapid drop in hardness as we move away from the weld. For example, while hardness decreases for all voltages, the reduction is steeper for 38 V in zones 5–6, which suggests that the higher voltage may result in greater thermal input, thus prolonging the cooling time in these areas and allowing for more pronounced microstructural changes. Interestingly, in zone 4, the hardness values are relatively similar across all three voltages, indicating that this may be a transitional area where the thermal effects of the weld are less dependent on the voltage applied.

After observing the resulting hardness for zone 2, a correlation can be made between the welding voltage used and the hardness value in the center of the cross-section of the weld bead. It is found that with the increase of the welding voltage, the hardness in zone 2 increases with an average step of approximately 1.1 HV/V.

In contrast, Figure 12 illustrates the hardness distribution along the Y-axis.

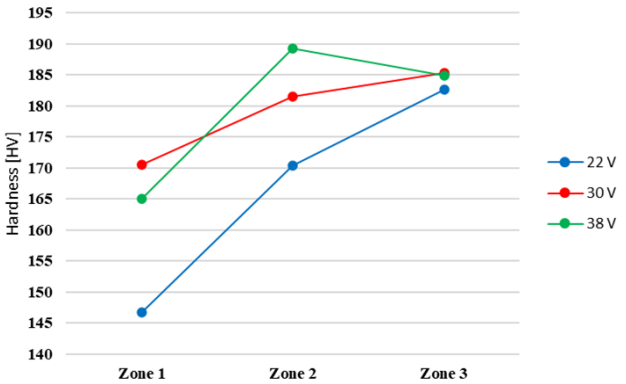

Figure 12 – Hardness distribution in the cross-section of the welding seam on the Y-axis

Hardness increases from zone 1 to zone 2 for all voltages, reaching a maximum in the heat-affected zone. For 38 V, this increase is the most pronounced, suggesting that higher voltage leads to more significant heat input, which can result in localized hardening due to rapid thermal transformations. After zone 2, there is a slight decrease in hardness as we approach zone 3. The trend shows that higher voltages like 38 V yield higher hardness in the central weld area, while 22 V results in generally lower hardness across all zones.

From these observations, it can be concluded that 38 V provides the highest hardness values in the welded joint, particularly in zone 2 along both axes, suggesting a more substantial hardening effect in this region. Zone 4 along the X-axis is notable as an area where hardness values converge, showing similar characteristics across all welding voltages. This indicates that in this specific zone, the effects of the welding voltage on hardness are minimized, likely due to the balance between heat input and cooling rates.

When analyzing the mechanical properties in terms of hardness, the 38 V welding mode offers the best potential for increased mechanical strength, as higher hardness typically correlates with improved wear resistance and tensile strength. However, the rapid hardness decrease observed in zones 5–6 for this voltage suggests that the higher heat input leads to slower cooling rates in the regions farther from the weld. This slower cooling process allows for more considerable grain growth, which can reduce hardness in these areas.

Conversely, the 22 V welding mode demonstrates a slower decrease in hardness, which might indicate a faster cooling rate in the heat-affected zone, leading to less significant microstructural changes. While this voltage may result in lower hardness overall, it could offer benefits in terms of ductility and reduced risk of brittle fracture, as excessively hardened areas can become more susceptible to cracking under stress.

Regarding cooling rates, regions closer to the weld, such as zone 2, are likely to experience faster cooling due to their proximity to the central heat source, resulting in higher hardness values. Areas farther from the weld, like Zones 5–6, may cool more slowly, especially at higher voltages (e.g., 38 V), prolonging the thermal cycle and reducing hardness.

Thus, 38 V provides the highest hardness in the weld and could offer advantages in applications requiring high wear resistance and mechanical strength. However, for a more balanced approach, where both hardness and ductility are essential, 30 V might offer the best compromise, with moderate hardness and less drastic changes in the heat-affected zone. Also, 22 V might be preferable where ductility and toughness are prioritized over extreme hardness. Thus, the optimal welding voltage depends on the specific mechanical requirements of the welded joint.

The variation in welding voltage significantly affects the overall characteristics of welded joints. Welding modes with higher voltage lead to more significant heat input, resulting in harder but more brittle welds, particularly in the central zones, with a sharper decrease in hardness toward the base material. Lower voltage modes produce softer joints with improved ductility but may not provide sufficient strength for high-stress environments. Moderate voltage modes offer a balanced profile and consistent hardness throughout, providing good mechanical strength without excessive brittleness and ensuring a more uniform and durable joint for long-term performance.

Based on the analysis of hardness distribution and the requirements for pressure vessels, the 30 V welding mode is recommended. It balances hardness and ductility, ensuring sufficient mechanical strength while minimizing the risk of brittle fractures. This mode promotes more uniform cooling, reducing extreme microstructural changes that could lead to failure under pressure or temperature variations. Therefore, 30 V provides optimal long-term performance for pressure vessels exposed to demanding operating conditions.

Looking at the influence of the welding voltage in terms of the dimensions of the welding seam, it can be noted that the increase of the welding voltage contributes to the much more pronounced dilution of the welding pool, a fact that favors the realization of welded joints with increased width. It is also possible to observe a slight tendency to decrease the height of the welding seam with the increase of the welding voltage.

In Figure 13, a variation of dimensions *W* and *H* (specified in Figure 10) is shown graphically, where the evolution of these 2D parameters depends on the welding voltage [38].

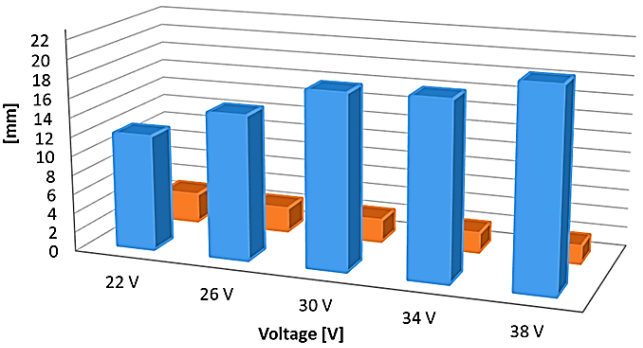

	22 V	26 V	30 V	34 V	38 V
Width of weld (W)	12	15	18.1	18.3	20.5
Height of weld (H)	3	2.5	2.3	2	1.8

Figure 13 – Evolution of welding seam dimensions *H* and *W* depending on the welding voltage

An aspect that should be mentioned is the fact that the penetration of the base material in the welding joint shows interruptions or even incomplete penetration along the entire length of the welded joint for some samples. This aspect is more pronounced for modes that use a higher welding voltage.

4.3 Microstructure analysis

The SEM micrographs (Figures 14–19) correspond to the six areas outlined in Figure 10, which represent specific zones within the welded joint of P355N material, joined using SAW technology.

Three different welding voltages were applied (22, 30, and 38 V), and the SEM analyses were conducted at two levels of magnification – 5000x for an overview and 20 000x for detailed phase identification. These images provide crucial insights into the microstructural evolution within the welded joint, HAZ, and the base material. The morphological and microstructural variations observed with different welding modes are critical for optimizing the welding parameters to ensure that the joints can withstand the operational requirements of pressure vessels, such as resistance to pressure, temperature variations, and long-term wear.

The analysis of the samples by category of welding modes from the point of view of the metallographic structure is treated by observing the structure in the six points presented in Figure 10.

In order to concentrate on the information, the welding modes that presented the values of the welding voltage 22, 33, and 38 V were selected for analysis, forming a set of images for each observed zone in which all three modes can be found.

After analyzing zone 1 using a magnitude of x5000, it can be noted the existence of grain formations that have a ferritic structure (labeled with F) inside, and the edges are formed by martensite-type solid bonds indicated by labeled with M, also at the magnitude of x20 000 smaller formations of bainitic phases can be observed among the martensitic structures (labeled with B). It is known that the cooling speed of molten metal mass directly influences the metallographic structures of steel. Similar visual images of the microstructure phases presented (F, M, and B) can also be found in other research, such as [39]. Figure 14 presents the evolution of area 1, located centrally in the joint.

The SEM images reveal the differences in microstructure resulting from the varying welding voltages. At 5000x magnification, the 22 V sample shows a fine-grained structure primarily composed of ferrite, with minimal bainite or martensite present. This suggests that the lower heat input during welding preserves a tougher, more ductile microstructure.

As the voltage increases to 30 V, bainite and martensite become more prominent, with grain coarsening beginning to appear. In the 38V sample, the microstructure is predominantly martensitic, with larger grains indicating higher hardness and increased brittleness.

At 20 000x magnification, the detailed phase distribution becomes clearer. In the 22 V sample, fine ferrite dominates the structure, with only small martensite regions contributing to good toughness and resistance to cracking. The 30 V sample shows more pronounced martensitic laths alongside bainite, compromising ductility but improving hardness. In the 38V sample, large, blocky martensitic structures dominate, indicating a brittle microstructure less suitable for high-stress environments like pressure vessels.

An essential role in the microstructural changes of the welded joint is also the cooling medium, in our case, the flux layer. It has the role of an insulator with the external environment from a thermal point of view, favoring the realization of a slower cooling that favors the appearance of ferrite in the structure of the material, this being a material with a low carbon content below 0.2 % forming hypo eutectoid metal structures consisting of a mixture ferrite and perlite.

Area 2 in the cross-section of the weld bead represents the core of the weld bead. Thus, it had the slowest cooling rate of all the areas present in the analysis, a fact that leads to the formation of ferritic-pearlitic structures according to the Fe-Fe_3C equilibrium diagram.

Figure 15 presents the microstructures collected in zone 2 at x5000 and x20 000 magnitudes.

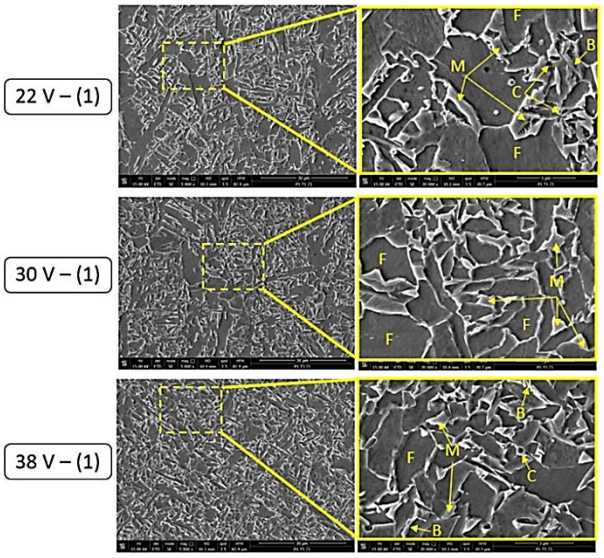

Figure 14 – SEM micrographs in the area 1

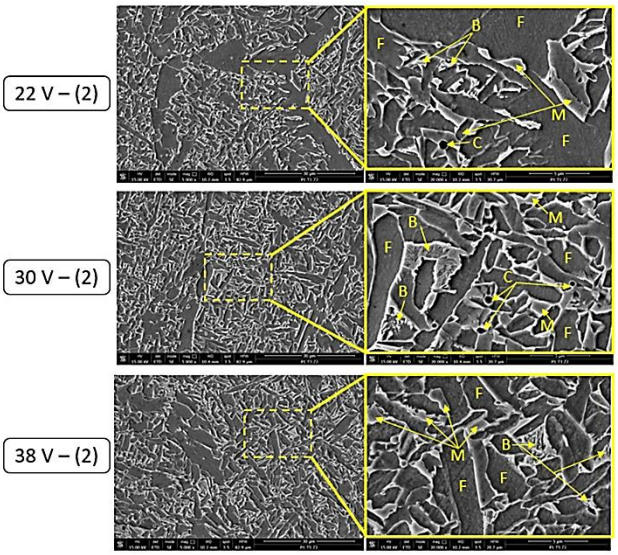

Figure 15 – SEM micrographs in the area 2

The micrographs collected at x5000 show that coarser ferritic grains are present in the welding performed at 22 V, compared to the welding modes performed at 30 V and 38 V.

At the x20 000 magnification for the welds made using 22 V welding mode, a remarkable ferrite zone, and concentrated bainitic formations infiltrated among the chains of martensitic structures can be noted.

At 5000x magnification, the 22 V sample displays a fine mixture of ferrite and bainite, with minimal heat-induced grain coarsening. The 30 V sample shows larger grains, with a greater presence of martensite and bainite, indicating that increased heat input leads to grain coarsening, which reduces toughness. The structure in the 38 V sample is mainly martensitic, with much coarser grains and fewer ferritic regions, indicating a loss of ductility and toughness.

At 20 000x magnification, the phase boundaries between ferrite and bainite in the 22 V sample are smooth and well-distributed, indicating good mechanical stability.

The 30 V sample shows more distinct martensitic laths, which increase hardness but reduce toughness. The martensite is very coarse in the 38 V sample, with few ferritic regions, suggesting a brittle structure more prone to cracking under operational stresses.

The microstructure of zone 3, which represents the upper part of the weld seam, is presented in Figure 16.

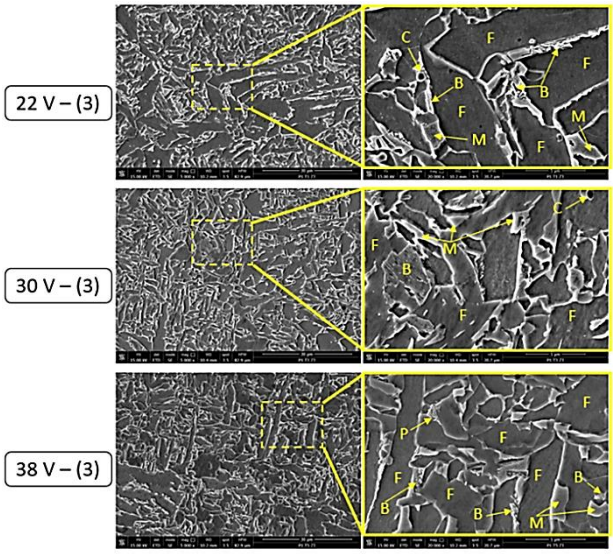

Figure 16 - SEM micrographs in the area 3

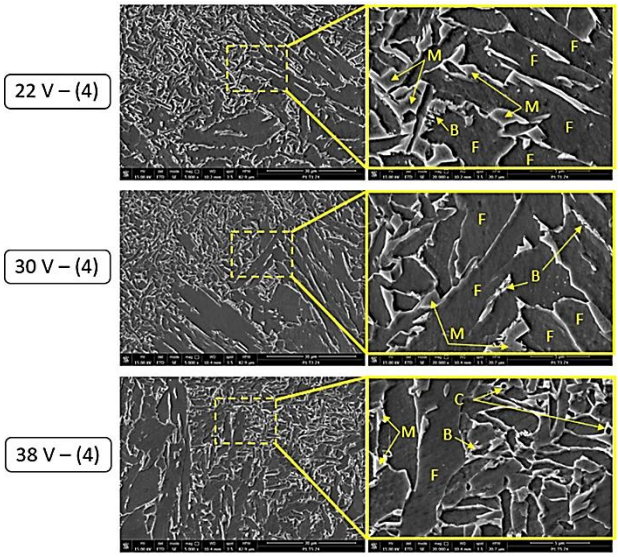

Figure 17 – SEM micrographs in the area 4

At a magnitude of x5000, it can be noted that the sample made with the welding voltage of 30 V shows the most abundant ferritic structures, making relatively large surfaces, and the sample that was made using welding voltages of 38 V, it shows at the same magnitude much smaller ferritic areas, having a much denser martensitic structure.

When analyzing each of the micrographs shown in Figure 16, it can be observed that large ferritic grains dominate the microstructure for the 22 V welding mode. Moreover, there are small networks of martensite and bainite, among which globular formations of carbides can also be noticed.

The sample made with a welding voltage of 30 V shows in area 3 at magnitudes of x20 000 martensitic and bainitic structures much more often than in the sample made with 22 V. An area with a bainitic structure can be noted in the form of relatively large precipitations compared to the other martensitic networks present.

In the case of the sample welded with a welding voltage of 38 V, a ferrite structure with martensitic edges can be noted, which in some places contain bainitic formations. The amount of ferrite is approximately the same as in the sample made with a welding voltage of 30 V.

Figure 17 shows the metallographic microstructures in area 4, the transition zone between the filler material and the base material of welded joints. At a magnitude of x5000, large ferrite regions and regions with very dense structures of martensitic edges with a ferritic core are visible.

In area 4, the 5000x magnification images show a fine-grained structure in the 22 V sample, with ferrite and bainite remaining dominant. Martensitic structures are more pronounced in the 30 V sample, indicating a shift towards higher hardness. The 38 V sample displays significant grain coarsening, with martensite dominating, which suggests a brittle microstructure that would be less able to absorb impact or stress.

At 20 000x magnification, the 22 V sample shows a consistent ferrite-bainite structure, ideal for maintaining toughness under operational conditions. However, the 30 V and 38 V samples show more significant martensitic content, with coarse grains and sharp boundaries that increase hardness but reduce toughness and ductility.

The images are more detailed at a magnitude of x20 000. It can be seen that the microstructure of area 4 presents the same phases as described for area 3, with some relatively large regions of ferrite being present and the rest having networks of martensitic structures with inserts of

bainitic structures in places. The microstructure corresponding to the sample welded with a welding voltage of 38 V indicates that carbides are also present at the magnitude of x20 000, and the martensitic structure has a higher density than in other modes (Figure 17).

After examining the microstructure in the thermally affected zone identified as zone 5 (Figure 18), it can be seen that at magnitudes of x5000, ferritic regions are in the base material, much more pronounced than in the previous zones, which have margins of martensitic regions with a uniform and repetitive character, forming elongated and grouped oriented grains in specific directions.

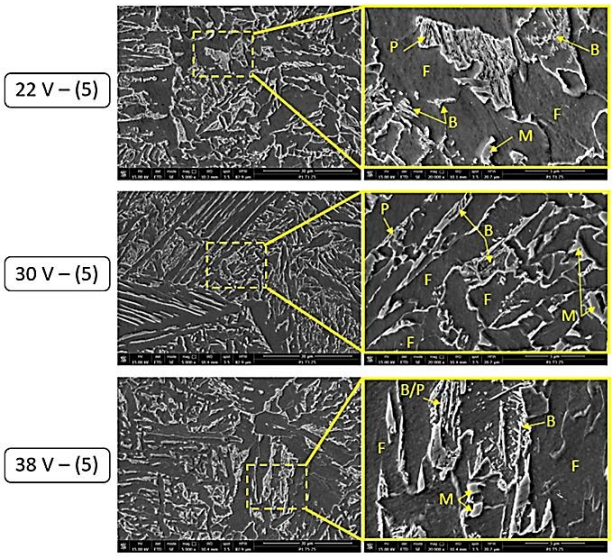

Figure 18 – SEM micrographs in the area 5

In area 5 at 5000x magnification, the 22V sample retains a fine, ferritic-bainitic structure. In the 30V sample, martensitic regions begin to dominate, and the 38V sample shows extensive coarsening, indicating reduced toughness and increased susceptibility to cracking.

At magnitudes of x20 000, it can observe the appearance of bainitic formations among the martensitic networks, which are the most pronounced in the welding mode made with 22 V, also observe a small structure with a pearlitic appearance being a lamellar interpenetration between ferrite and martensite.

The 22 V sample maintains fine phase boundaries, suggesting excellent mechanical properties, while the 30V and 38 V samples show increasingly larger martensitic regions, reducing the material's resistance to long-term stress.

Finally, Figure 19 shows the microstructure of the base material at magnitudes of x5000 and x20 000, where martensitic and bainitic phase bonding patterns form a microstructure in which the ferritic phase is predominant.

Within the microstructure of the base material, the dominant formations are the majority formations bordered by martensitic boundaries around which considerable bainitic structures can be found. The material presented suitable plastic and tenacity properties, which is demonstrated by how the samples for the tensile test broke. Those that had a fully penetrated and strong welded joint were broken through the base material with a significant stretching until breaking (the case of the welded samples using 22, 33, and 38 V).

The SEM analysis across various magnifications and areas shows that the welding mode plays a critical role in determining the microstructure of the welded joints.

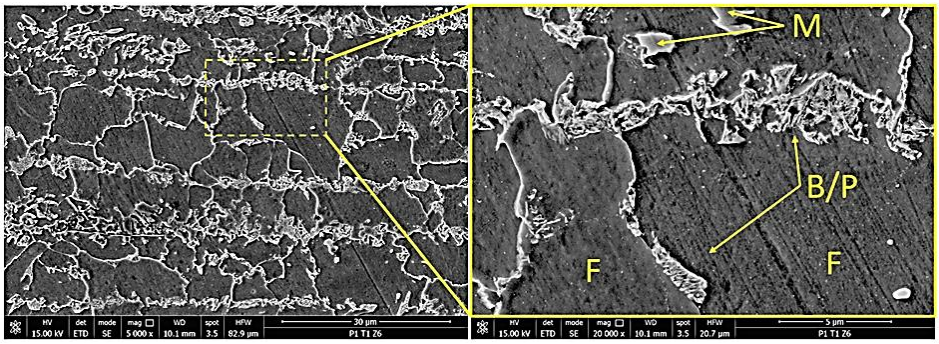

Figure 19 – SEM micrographs in the area 6

The 22 V welding voltage consistently produces finer, more balanced microstructures across the weld, HAZ, and base material. This fine ferrite-bainite structure offers superior toughness, ductility, and resistance to cracking, making it the most suitable for pressure vessel applications. In contrast, the 30 V and 38 V modes result in coarser, martensitic-dominated structures, which increase hardness but at the cost of toughness and flexibility, making them less ideal for long-term performance under fluctuating stress and temperature conditions.

5 Discussion

After analyzing the images magnified at x20 000 (Figure 14), martensitic substructures indicated with the letter M can be observed, these being recognized by their smooth and bright appearance just as they are presented in other research works [40, 41]. Most of the phases bordered by the martensitic boundaries are the ferritic ones, which have a smooth gray appearance indicated by the letter F.

Other structures present are the bainitic type, which the appearance of martensitic structures with precipitation and discontinuous shapes like a bumpy relief can identify. They are indicated with the letter B and are present in

smaller quantities than the martensitic structures. The last element noted in the microstructure is carbide, indicated by the letter C, and is recognized by the presence of concentrated globules with a round shape smaller than the previously mentioned structures [41].

From Figure 15, in the case of the sample made using the value of the welding voltage of 30 V, it was noted at the magnitude of x20 000 the appearance of several carbides and the presence of a considerable area that can be identified as a bainitic structure, the rest of the structures being martensitic boundaries between which there are ferritic structures [42].

On the metallographic sample specific to the welding mode, which is characterized by the welding voltage of 38 V, the presence of dense martensite structures bordering relatively uniform ferritic zones in terms of shape and volume was noted at a magnitude of x20 000, the presence of a pronounced bainitic zone is also noted in the form of a square and other small and isolated areas also bainitic [43].

For pressure vessels that should resist pressure variations, temperature fluctuations, and long-term wear due to corrosion or fatigue, the 22V mode is optimal. It balances mechanical strength and toughness well, ensuring the integrity and durability of the welded joints in harsh operational environments [44–46].

6 Conclusions

The experimental investigation of welding voltages on 6 mm thick P355N material using submerged arc welding technology revealed significant differences in the microstructural and mechanical performance of the welded joints. The effects were studied through tensile testing, hardness measurements, dimensional inspection, and microstructural analysis across three welding modes: 22, 30, and 38 V.

The main conclusions of each set of tests are the following. First, the 22 V welding mode performed best in tensile tests, producing the highest tensile strength and ductility. The 30V and 38V modes exhibited reduced ductility, with the 38V mode showing the highest strength but the lowest ability to withstand stretching before fracture, indicating increased brittleness.

Second, the hardness results showed that the 38 V mode produced the hardest welds, with high values concentrated in the weld zone but with a steep drop toward the base material, suggesting lower overall toughness. The 22 V mode provided a more even hardness distribution, ensuring a balanced performance between hardness and ductility, which is critical for pressure vessel applications.

Third, from a dimensional perspective, higher welding voltages (30 and 38 V) resulted in broader and more pronounced weld seams but incomplete penetration and irregularities along the joint. In contrast, the 22 V mode produced a visually consistent and smoother weld profile, with fewer imperfections and better overall geometry, favoring its use for critical applications.

Moreover, the microstructural evaluation revealed that the 22 V mode led to a fine-grained structure, predominantly composed of ferrite and bainite, with minimal martensitic formation. This results in a more ductile and less brittle joint, whereas the 30V and 38V modes introduced higher levels of martensite, leading to increased hardness but reduced toughness, particularly in the 38V mode.

Overall, after considering the performance in all tests, the 22 V welding mode is the optimal choice for welding 6 mm thick P355N plates, especially for pressure vessel applications. It best balances tensile strength, hardness, dimensional stability, and microstructural toughness, ensuring long-term durability and resistance to operational stresses such as pressure variations and temperature changes.

References

1. Moss, D.R. (2004). *Pressure Vessel Design Manual* (3rd ed.). Gulf Professional Publishing, Houston, TX, USA.
2. Prasanth, D., Sachidananda, H.K. (2019). Design and analysis of pressure vessel. *International Journal of Mechanical and Production Engineering Research and Development*, Vol. 9(5), pp. 125–136.
3. Lin, P.D., Nie, J.F., Cui, W.D., He, L., Lu, Y., Cui, S. (2024). A multiscale study on the microstructure and hardening models of the irradiation defects on reactor pressure vessel steels: Modelling and experiment. *Journal of Materials Research and Technology*, Vol. 30, pp. 520–531. https://doi.org/10.1016/j.jmrt.2024.03.028
4. Karaoğlu, S., Seçgin, A. (2008). Sensitivity analysis of submerged arc welding process parameters. *Journal of Materials Processing Technology*, Vol. 202, pp. 500–507. https://doi.org/10.1016/j.jmatprotec.2007.10.035
5. Kanjilal, P., Pal, T.K., Majumdar, S.K. (2006). Combined effect of flux and welding parameters on chemical composition and mechanical properties of submerged arc weld metal. *Journal of Materials Processing Technology*, Vol. 171(2), pp. 223–231. https://doi.org/10.1016/j.jmatprotec.2005.06.083
6. Ahmad, M.A., Sheikh, A.K., Nazir, K. (2019). Design of experiment-based statistical approaches to optimize submerged arc welding process parameters. *Journal of Materials Processing Technology*, Vol. 94, pp. 307–315. https://doi.org/10.1016/j.isatra.2019.04.003
7. Zhang, L. (2023). Effect of process parameters on the formability, microstructure, and mechanical properties of laser-arc hybrid welding of Q355B steel. *Materials*, Vol. 16(12), 4253. https://doi.org/10.3390/ma16124253
8. Assefa, A.T., Ahmed, G.M.S., Alamri, S., Edacherian, A., Jiru, M.G., Pandey, V., Hossain, N. (2022). Experimental investigation and parametric optimization of the tungsten inert gas welding process parameters of dissimilar metals. *Materials*, Vol. 15(13), 4426. https://doi.org/10.3390/ma15134426

9. Habba, M.I.A., Alsaleh, N.A., Badran, T.E., El-Sayed Seleman, M.M., Ataya, S., El-Nikhaily, A.E., Abdul-Latif, A., Ahmed, M.M.Z. (2023). Comparative study of FSW, MIG, and TIG welding of AA5083-H111 based on the evaluation of welded joints and economic aspect. *Materials*, Vol. 16(14), 5124. https://doi.org/10.3390/ma16145124
10. Ziółkowski, W., Boroński, D., Skibicki, A., Stachowiak, R., Kosturek, R., Śnieżek, L. (2023). Mechanical properties and microstructure of dissimilar S355/AA6061-T6 FSW butt joints. *Materials*, Vol. 16(17), 5950. https://doi.org/10.3390/ma16175950
11. Peasura, P. (2017). Investigation of the effects of submerged arc welding process parameters on the mechanical properties of pressure vessel steel ASTM A283 Grade A. *Journal of Engineering*, Vol. 2017, 9048324. https://doi.org/10.1155/2017/9048324
12. Ramakrishnan, M., Muthupandi, V. (2013). Application of submerged arc welding technology with cold wire addition for drum shell long seam butt welds of pressure vessel components. *International Journal of Advanced Manufacturing Technology*, Vol. 65, pp. 945–956. https://doi.org/10.1007/s00170-012-4230-0
13. Takeuchi, T., Kameda, J., Nagai, Y., Toyama, T., Matsukawa, Y., Nishiyama, Y., Onizawa, K. (2012). Microstructural changes of a thermally aged stainless steel submerged arc weld overlay cladding of nuclear reactor pressure vessels. *Journal of Nuclear Materials*, Vol. 425(1–3), pp. 60–64. https://doi.org/10.1016/j.jnucmat.2011.12.004
14. Cioroagă, B.D., Linul, E., Cioată, V.G. (2023). Effect of welding speed on tensile strength of pressure vessel steel submerged welded joints. *Annals of Faculty Engineering Hunedoara – International Journal of Engineering*, Vol. XXI, pp. 93–96.
15. Cioroagă, B.D., Socalici, A.V., Cioată, V.G., Dascăl, A.A., Ardelean, M. (2023). Analysis of electric flux arc welding parameters influence using visual X-ray inspection. *Materials Today: Proceedings*, Vol. 78(2), pp. 214–220. https://doi.org/10.1016/j.matpr.2022.10.107
16. Cioroagă, B.D., Cioată, V.G. (2023). X-ray analysis of welding parameters influence on pressure vessel steel P355 N. *Journal of Physics: Conference Series*, Vol. 2540, 012040. https://doi.org/10.1088/1742-6596/2540/1/012040
17. Ebrahimi, A., Babu, A., Kleijn, C. R., Hermans, M. J. M., Richardson, I. M. (2021). The effect of groove shape on molten metal flow behaviour in gas metal arc welding. *Materials*, Vol. 14(23), 7444. https://doi.org/10.3390/ma14237444
18. Murugan, N., Gunaraj, V. (2005). Prediction and control of weld bead geometry and shape relationships in submerged arc welding of pipes. *Journal of Materials Processing Technology*, Vol. 168, pp. 478–487. https://doi.org/10.1016/j.jmatprotec.2005.03.001
19. Manonmani, K., Murugan, N., Buvanasekaran, G. (2007). Effects of process parameters on the bead geometry of laser beam butt welded stainless steel sheets. *International Journal of Advanced Manufacturing Technology*, Vol. 32, pp. 1125–1133. https://doi.org/10.1007/s00170-006-0432-7
20. He, W., Zhang, A., Wang, P. (2023). Weld cross-section profile fitting and geometric dimension measurement method based on machine vision. *Applied Sciences*, Vol. 13(7), 4455. https://doi.org/10.3390/app13074455
21. Dong, P., Li, H., Sun, D., Gong, W., Liu, J. (2013). Effects of welding speed on the microstructure and hardness in friction stir welding joints of 6005A-T6 aluminum alloy. *Materials & Design*, Vol. 45, pp. 524–531. https://doi.org/10.1016/j.matdes.2012.09.040
22. Gharibshahiyan, E., Raouf, A.H., Parvin, N., Rahimian, M. (2011). The effect of microstructure on hardness and toughness of low carbon welded steel using inert gas welding. *Materials & Design*, Vol. 32, pp. 2042–2048. https://doi.org/10.1016/j.matdes.2010.11.056
23. Singh, R.P., Singh, A., Singh, A. (2020). Optimization of hardness of weld in submerged arc welding. *Materials Today: Proceedings*, Vol. 26(2), pp. 1827–1830. https://doi.org/10.1016/j.matpr.2020.02.382
24. Küçüköner, H., Karakoç, H., Kahraman, N. (2020). Investigation of microstructure and mechanical properties of AISI2205/DIN-P355GH steel joint by submerged arc welding. *Journal of Manufacturing Processes*, Vol. 59, pp. 566–586. https://doi.org/10.1016/j.jmapro.2020.10.023
25. Lan, L., Qiu, C., Zhao, D., Gao, X., Du, L. (2020). Analysis of microstructural variation and mechanical behaviors in submerged arc welded joint of high strength low carbon bainitic steel. *Materials Today: Proceedings*, Vol. 26, pp. 1931–1935. https://doi.org/10.1016/j.msea.2012.08.057
26. European Committee for Standardization (2005). *EN 10027-1:2005, Designation systems for steels – Part 1: Steel names*. Brussels, Belgium.
27. European Committee for Standardization (2014). *EN 10216-3:2014, Seamless steel tubes for pressure purposes. Technical delivery conditions. Alloy fine grain steel tubes*. Brussels, Belgium.
28. ESAB (2019). *Technical Handbook, Submerged Arc Welding – Fluxes and Wires for Joining Non and Low-Alloyed Steels, Stainless Steels and Nickel-Base Alloys*. ESAB, Gothenburg, Sweden.
29. European Committee for Standardization (2009). *EN ISO 4063:2009, welding and allied processes – Nomenclature of processes and reference numbers*. Brussels, Belgium.
30. European Committee for Standardization (2011). *SR EN 287-1:2011, Qualification test of welders – Fusion welding Part 1: Steels.* Brussels, Belgium.
31. European Committee for Standardization (2011). *SR EN ISO 6947:2011, welding and allied processes – Welding positions.* Brussels, Belgium.
32. Murugan, N., Gunaraj, V. (2005). Prediction and control of weld bead geometry and shape relationships in submerged arc welding of pipes. *Journal of Materials Processing Technology*, Vol. 168(3), pp. 478–487. https://doi.org/10.1016/j.jmatprotec.2005.03.001

33. British Standards Institution (1995). *BS EN 895:1995, Destructive tests on welds in metallic materials – transverse tensile test.* Milton Keynes, United Kingdom.
34. Zhang, T., Ji, H., Xu, D., Yin, X., Wei, H., Sun, Z., Liu, C. (2023). A hybrid shoulder to achieve a significant improvement in tensile strength and fatigue performance of friction stir welded joints for Al–Mg–Si alloy. *Journal of Materials Research and Technology*, Vol. 23, pp. 3791–3804. https://doi.org/10.1016/j.jmrt.2023.10.067
35. Conte, R., Battista, F.R., Ambrogio, G. (2024). Submerged arc welding process: enhancement of production performance based on metallurgical observations. *The International Journal of Advanced Manufacturing Technology*, Vol. 134, 781–793. https://doi.org/10.1007/s00170-024-14153-y
36. Kosturek, R., Torzewski, J., Wachowski, M., Śnieżek, L. (2022). Effect of welding parameters on mechanical properties and microstructure of friction stir welded AA7075-T651 aluminum alloy butt joints. *Materials*, Vol. 15(17), 5950. https://doi.org/10.3390/ma15175950
37. Gunaraj, V., Murugan, N. (2000). Prediction and optimization of weld bead volume for the submerged arc process - Part 2. *Journal of Materials Processing Technology*, Vol. 88, pp. 266–275.
38. European Committee for Standardization (2001). *EN 1011-2:2001, Welding – Recommendations for welding of metallic materials – Part 2: Arc welding of ferritic steels.* Brussels, Belgium.
39. Şenol, M., Çam, G. (2023). Investigation into microstructures and properties of AISI 430 ferritic steel butt joints fabricated by GMAW. *International Journal of Pressure Vessels and Piping*, Vol. 202, 104926. https://doi.org/10.1016/j.ijpvp.2023.104926
40. Torres-Treviño, L.M., Reyes-Valdes, F.A., López, V., Praga-Alejo, R. (2011). Multi-objective optimization of a welding process by the estimation of the Pareto optimal set. *Expert Systems with Applications*, Vol. 38(7), pp. 8045–8053. https://doi.org/10.1016/j.eswa.2010.12.139
41. Bellamkonda, P.N., Dwivedy, M., Addanki, R. (2024). Cold metal transfer technology – A review of recent research developments. *Results in Engineering*, Vol. 23, 102423. https://doi.org/10.1016/j.rineng.2024.102423
42. Rao, R.V., Rai, D.P. (2017). Optimization of submerged arc welding process parameters using quasi-oppositional based Jaya algorithm. *Journal of Mechanical Science and Technology*, Vol. 31, pp. 2513–2522 (2017). https://doi.org/10.1007/s12206-017-0449-x
43. Chandel, R.S., Seow, H.P., Cheong, F.L. (1998). Effect of increasing deposition rate on the bead geometry of submerged arc welds. *Welding Journal*, Vol. 72(1), pp. 124–128. https://doi.org/10.1016/S0924-0136(97)00139-8
44. Dhas, J.E.R., Kumanan, S. (1998). Optimization of parameters of submerged arc weld using non conventional techniques. *Applied Soft Computing*, Vol. 11(8), pp. 5198–5204. https://doi.org/10.1016/j.asoc.2011.05.041
45. Kah, P., Suoranta, R., Martikainen, J., Magnus, C. (2014). Techniques for joining dissimilar materials: Metals and polymers. *Reviews on Advanced Materials Science*, Vol. 36, pp. 152–164.
46. Selamat, N.F., Ishak, M., Muhamad, M.R., Sulong, M.Z., Harun, Z., Hasbullah, S.A. (2020). Optimization of process parameters of submerged arc welding by Taguchi method. *Materials Today: Proceedings*, Vol. 47(19), pp. 7067–7072. https://doi.org/10.1016/j.matpr.2021.06.141